

Correlation effects on 3D topological phases: from bulk to boundary

Ara Go,^{1,2} William Witczak-Krempa,³ Gun Sang Jeon,² Kwon Park,⁴ and Yong Baek Kim^{3,4}

¹*Department of Physics and Astronomy and Center for Theoretical Physics,
Seoul National University, Seoul 151-747, Korea*

²*Department of Physics, Ewha Womans University, Seoul 120-750, Korea*

³*Department of Physics, University of Toronto, Toronto, Ontario M5S 1A7, Canada*

⁴*School of Physics, Korea Institute for Advanced Study, Seoul 130-722, Korea*

(Dated: September 10, 2021)

Topological phases of quantum matter defy characterization by conventional order parameters but can exhibit quantized electro-magnetic response and/or protected surface states. We examine such phenomena in a model for three-dimensional correlated complex oxides, the pyrochlore iridates. The model realizes interacting topological insulators with and without time-reversal symmetry, and topological Weyl semimetals. We use cellular dynamical mean field theory, a method that incorporates quantum-many-body effects and allows us to evaluate the magneto-electric topological response coefficient in correlated systems. This invariant is used to unravel the presence of an interacting axion insulator absent within a simple mean field study. We corroborate our bulk results by studying the evolution of the topological boundary states in the presence of interactions. Consequences for experiments and for the search for correlated materials with symmetry-protected topological order are given.

The interplay of symmetry and topology has recently proven a rich avenue for the discovery of new phases of matter, some of which have been experimentally identified. A recent example is the prediction and subsequent observation of topological insulators (TIs) preserving time-reversal symmetry (TRS) [1, 2]. The symmetry-protected topological orders in such phases cannot be fully characterized by conventional order parameters. They can, however, display universal electromagnetic response and/or robust boundary states. This follows from the presence of non-trivial quantum entanglement in the ground state of these phases [3]. In TRS-protected topological band insulators, such order can be characterized by a topological invariant in terms of the single-particle wavefunction[1]. This approach cannot be applied in the presence of interactions. Rather, one can ask if the correlated material exhibits a universal and quantized physical response to a given external perturbation. For three-dimensional (3D) TIs, the quantized response is the magneto-electric effect [4], according to which an externally applied electric field on the sample generates a parallel magnetic field, and vice versa, with the response coefficient depending solely on universal constants. It was argued on the grounds of topological field theory that the magneto-electric effect remains a well-defined topological response in the presence of interactions [5]. Moreover, a topological index was given in terms of the full interacting electronic Green's function. As some of the considerations in the establishment of such an invariant are rather abstract, it would be desirable to have a concrete verification of such an important claim.

We calculate this topological invariant within a strongly correlated electronic Hamiltonian by means of cellular dynamical mean-field theory (CDMFT) [6, 7], which gives access to the Green's function of the inter-

acting electrons. This index allows us to determine the presence of correlated topological insulators, with and without TRS (here, the latter case corresponds to an axion insulator), and their breakdown for sufficiently large correlations.

A complementary aspect of the quantized magneto-electric effect is the presence of protected surface states, which we verify by analysing our interacting model in a finite-slab geometry. We do find that the TI surface states are robust to interactions, thus establishing the bulk-boundary connection for an interacting system and providing a check for the non-trivial topological index. Further, the surface state analysis allows us to study correlation effects on a closely related gapless phase: the topological Weyl semimetal, which has Weyl-fermion excitations and non-trivial surface states [8–11].

We use a model relevant to a class of 3D complex oxides, the pyrochlore iridates[8, 12–15]. These materials, and closely related Iridium-based compounds, are currently under close experimental scrutiny due to recent proposals for topological phases [8, 12–16]. As correlations seem important in these d -electron compounds, our work can be instrumental in their analysis. However, we emphasize that as we are dealing with topological phases, many of our results are expected to hold in general. Indeed, we envision that our methods can be fruitfully used in the analysis of correlated symmetry-protected topological ordered states and combined with *ab initio* tools in the quest for experimentally relevant candidate materials [17].

Model: The pyrochlore iridates, $R_2\text{Ir}_2\text{O}_7$, are 3D complex oxides where R is Yttrium or a rare earth. In many instances R is non-magnetic and the physics is mainly dictated by Iridium's (Ir) $5d$ -electrons. Due to the larger extent of the $5d$ atomic orbitals (compared with $3d$), the

energy scales associated with spin-orbit coupling and local repulsion are comparable. This sets the stage for the interplay between band topology and Mott physics. A microscopically-tailored model that captures this interplay is the following Hubbard Hamiltonian for the $5d$ -electrons hopping on the Iridium pyrochlore lattice with onsite Coulomb repulsion [15]:

$$H = \sum_{\langle \mathbf{R}i, \mathbf{R}'i' \rangle, \sigma\sigma'} ([T_o]_{ii'}^{\sigma\sigma'} + [T_d]_{ii'}^{\sigma\sigma'}) c_{\mathbf{R}i\sigma}^\dagger c_{\mathbf{R}'i'\sigma} - \mu \sum_{\mathbf{R}i, \sigma} c_{\mathbf{R}i\sigma}^\dagger c_{\mathbf{R}i\sigma} + U \sum_{\mathbf{R}i} n_{\mathbf{R}i\uparrow} n_{\mathbf{R}i\downarrow}, \quad (1)$$

where $c_{\mathbf{R}i\sigma}$ annihilates an electron with pseudospin σ at the i th basis site of the Bravais lattice vector \mathbf{R} . The index i runs from 1 to 4 and labels the corners of a tetrahedron. The hopping matrix T_o arises from oxygen-mediated hopping between the Ir atoms [12] with amplitude t , while T_d from the Ir-Ir hopping due to the *direct* overlap between the extended $5d$ -orbitals. The latter depends on two energy scales, t_σ and t_π , arising from the σ - and π -bonding between the orbitals, respectively. The chemical potential, μ , is such that each Ir atom contributes a single pseudospin-1/2 electron. The pseudospin arises from the combined effect of crystal fields and spin-orbit coupling [18]. Finally, the Hubbard repulsion U generates correlations by penalizing double occupation and thus drives the system away from simple single-particle physics. (We shall use the oxygen-mediated hopping amplitude, t , as our comparison scale.)

The phase diagram of the above Hamiltonian was previously analyzed by treating the onsite repulsion within a mean-field Hartree-Fock (HF) approach [15], which allows for a single-particle description. It was found that for small U/t , one obtains topological insulator and metallic phases, depending on the ratios t_σ/t and t_π/t . At sufficiently large U , the systems become magnetic. Near the magnetic transitions, it was found that topological Weyl semimetals (TWS) arise. Here, we shall focus on a representative set of hopping parameters: $t_\sigma/t = 1$, with the ratio $t_\pi/t_\sigma = -2/3$ fixed. In that case, the HF mean-field theory predicts that the system undergoes successive transitions from a TI to a TWS, and to an antiferromagnetic insulator (AFI) as one increases U . It is worth noting that the same succession of phases can be found within the HF framework for $t_\sigma/t < -1.67$, and we thus expect that the results we present below can be applied there as well. A detailed study of the full phase diagram is left for future work.

We use the above model to examine the fate of these phases and transitions within CDMFT. This method has been widely used to investigate correlated microscopic models [7] but only recently was it applied to topological phases [19], specializing to two dimensions. We emphasize that CDMFT fully incorporates the quantum many-

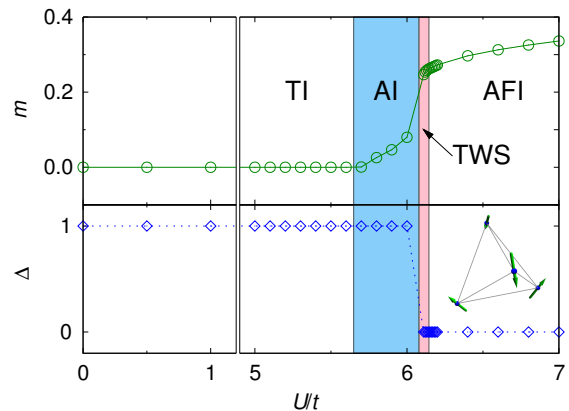


FIG. 1. Magnetization (m) and topological index (Δ) versus interaction strength. An interaction-driven topological transition accompanies an abrupt change of the magnetization. In the intermediate region, a topologically nontrivial insulator with a finite magnetization indicates the realization of an interacting axion insulator (AI). As the interaction strength increases, a topological Weyl semimetal (TWS) appears after the magnetization jump. At large U , the system is a topologically-trivial antiferromagnetic insulator (AFI). The magnetic structure is illustrated in the inset.

body effects within a cluster (unit cell here).

The phase diagram together with the magnetization and topological index are shown in Fig. 1. After the magnetization jumps, a topological Weyl semimetal emerges, as we establish from the spectral properties of the surface (Fig. 2) and bulk (Fig. 3) states. The \mathbb{Z}_2 index, Δ , determines the presence of a quantized magneto-electric response. Specifically, $\Delta = 1$ implies that an applied electric field \mathbf{E} will induce a magnetization in a properly prepared system: $\mathbf{M} = \alpha \mathbf{E}$, where $\alpha = e^2/2h$ depends only on universal constants [4]. In the presence of TRS, this topological response can be used as a defining property of a correlated TI. The associated \mathbb{Z}_2 topological index can be computed from the full interacting Green's function by a Wess-Zumino-Witten like integral [5]. It has been shown recently that in the special case where inversion symmetry is present, as is the case in this work, one can use a simplified criterion [20]:

$$(-1)^\Delta = \prod_{\mathbf{R}\text{-zero}} \eta_\alpha^{1/2}, \quad (2)$$

where $\eta_\alpha = \pm 1$ is a parity eigenvalue corresponding to a vector $|\alpha\rangle$, an *eigenstate of the interacting Green's function* evaluated at one of eight special momenta, Γ_i . These are the time reversal invariant momenta (TRIM) satisfying $-\Gamma_i = \Gamma_i$, up to a reciprocal lattice vector. Equation (2) is in contrast with the analogous Fu-Kane formula which can only be used for non-interacting systems. More details about Δ , such as the definition of “R-zero” (which reduces to that of an occupied band in the non-interacting limit), can be found in the Supplementary

Material and in [20].

From Fig. 1, we can see that the invariant indicates the presence of a topologically non-trivial phase for a wide range of onsite repulsion until a trivial phase results in the magnetic antiferromagnet, found at large U . It can be noted that the topological index remains invariant irrespective of the evolution of the Green's function due to interactions, which can be seen from the broadening of the spectral function, for instance. Eventually, TRS is broken, and there is a quantum phase transition out of the TI. From Fig. 1, we note that there is a regime where the magnetization increases continuously from zero before jumping discontinuously at $U/t = 6.11$. The latter jump, where the order parameter has a sudden increase although TRS has already been broken, signals a first order transition. We have verified that it is a robust property within our framework. Figure 1 shows that the range where the magnetization increases continuously from zero has $\Delta = 1$. Because of the breaking of TRS, one cannot identify this as a TI in the above sense. Rather it is a closely-related phase: a *correlated axion insulator*. It was introduced at the non-interacting level by Refs. [8, 21], where it was noted that even in the absence of TRS, by virtue of inversion symmetry and a special structure of the parity eigenvalues, the topological magneto-electric effect discussed above could be realized. Contrary to the TI, this phase does not have protected boundary states. As we argue in the Supplementary Material, the Δ -invariant, Eq. (2), is a natural generalization of the one introduced in Refs. [21, 22] as it counts the total number of odd-parity eigenstates, not only one per Kramers pair. We add that one expects such a phase to be present if the magnetization increases continuously from a TI, because the parity structure is not expected to change dramatically. Finally, as the continuous transition preceding the first order one is a feature that is absent from the HF mean-field theory, this axion phase is fundamentally correlation driven.

Surface states: Another route to examining the non-trivial topology of the ground state is via the bulk-boundary correspondence which, at the non-interacting level, guarantees the existence of protected surface states on any boundary with a trivial insulator, such as the vacuum. We verify this correspondence at the interacting level by performing a real space CDMFT calculation [19] on a slab that is finite along one direction. We solve for the layer-dependent Green's function self-consistently. The Supplementary Material contains details regarding the slab calculation.

The spectral function plotted in Fig. 2(c) shows that the topological surface states persist as correlations are increased, the latter leading to spectral broadening and to the appearance of high energy states. Eventually the slab system undergoes a first order transition to a TWS. At large U , we have an AFI without any spectral weight in the gap coming from the boundaries. Note that the

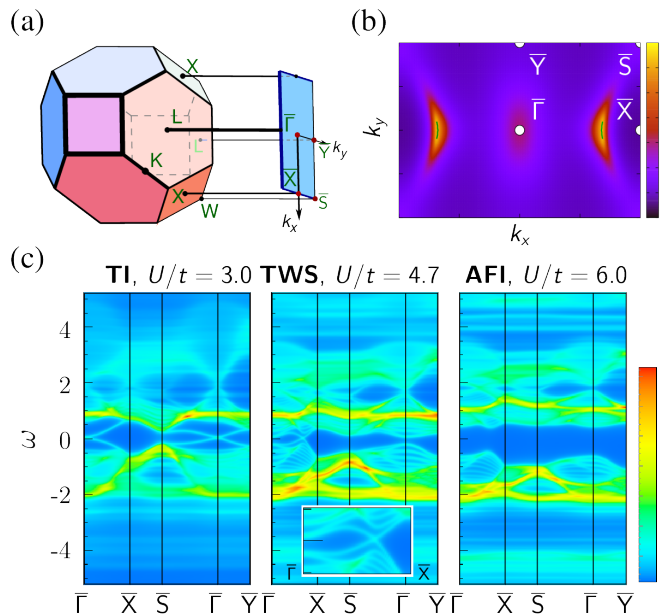


FIG. 2. Surface states of a slab normal to (110). (a) First Brillouin zone (BZ) of a pyrochlore lattice and its projection onto the (110)-surface BZ. (b) Spectral weight at the Fermi level, $\omega = 0$, for the TWS with $U/t = 4.7$. Fermi arcs crossing $k_y = 0$ clearly appear. The position of the arcs is roughly consistent with the HF result, denoted by green lines. (c) Density plot of the surface spectral functions along lines connecting high-symmetry points. From left to right, the panels represent a topological insulator (TI), a topological Weyl semimetal (TWS), and an antiferromagnetic insulator (AFI). The inset shows more clearly the surface states of the TWS near the Fermi level, $\omega = 0$.

axion insulating phase presented in the above discussion for the bulk Hamiltonian is absent for the slab as there is no continuous rise of the magnetization. We attribute this to the finiteness of the system in one direction and expect the continuous transition to be recovered as one introduces more layers.

Correlated topological Weyl semimetal: After the magnetization jump in Fig. 1, the spectral gap closes and one obtains a region of TWS before the AFI at large U . The topological Weyl semimetal, as introduced at the non-interacting level [8], is a gapless state with a Fermi surface consisting of (Weyl) points around which the dispersion is linear. These points are topologically robust as no local perturbation can gap them, as long as two Weyl points of opposite chirality do not mix. The protection of the Weyl node comes from the fact that only two bands meet at a point in three dimensions: all Pauli matrices have been used in the Hamiltonian of the Weyl point and an additional perturbation can only move the touching in the Brillouin zone (BZ). A fingerprint of the singular dispersion of the TWS is that it harbors protected surface states which take the form of Fermi arcs in the surface BZ [8].

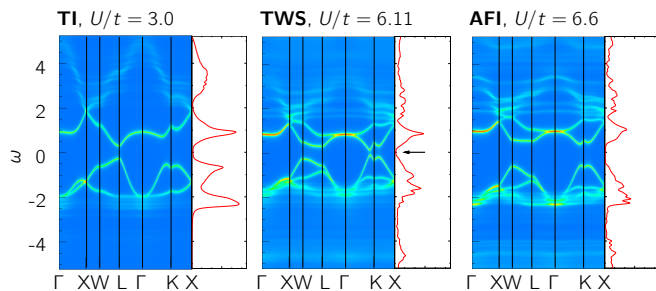


FIG. 3. Spectral weights along high symmetry lines and local density of states for different values of U/t . The panels represent a TI, a TWS, and an AF insulator. These last two phases break TRS. In the TWS, the Weyl points are not along high symmetry lines, but the density of states shows a quadratic scaling indicating their presence, as shown by the arrow.

At the level of the bulk calculation, we have determined that the spectral gap closes and the density of states shows a quadratic vanishing at the Fermi level ($\omega = 0$), Fig. 3, as is expected from linearly dispersing fermions in 3D. The eight Weyl points are not along high symmetry directions, hence Fig. 3 does not show the states of interest. A decisive signature of the correlated Weyl phase comes from the surface state calculation. We again consider a slab with surfaces normal to the (110) direction. We find clear Fermi arcs arising from states localized on the surfaces as we show in Fig. 2(b). The arcs are broadened compared to the sharp lines found at the non-interacting level. From the non-interacting theory we know that the arcs should join the projected bulk Weyl points on the surface BZ. Moreover, if for a given surface two Weyl points of opposite chirality are projected onto each other, no Fermi arc should arise from that point. In Fig. 2(b), only two arcs can be seen for two reasons: first, the arcs coming from the top and bottom surfaces overlap too much to be distinguished; second, two pairs of opposite chirality are annihilated upon projection. We thus establish that the rule for the projection holds in the correlated phase, i.e. the notion of chirality for the quasiparticles persists.

Discussion: We have so far mainly focused on theoretical studies of correlation effects on topological phases such as topological insulators and Weyl semimetals. Indeed, we have established the robustness of TIs from both sides of the bulk-boundary duality. A bulk topological invariant defined in terms of interacting Green's functions was explicitly evaluated. We determined its change at a correlation driven topological transition to a trivial AF insulator. This invariant was used to predict the existence of a correlated axion phase at the onset of a continuous magnetic transition. From the boundary perspective, our work has shown that the surface states of both TIs and topological Weyl semimetals remain robust to interactions.

We now turn to the experimental considerations. The model we used is applicable to a large class of complex oxides, the pyrochlore iridates. These show metal-insulator transitions as the rare earth is changed [23] or pressure [24] applied. There are indications that some members of the family magnetically order at low temperatures [25–29]. However, it is still not clear what the nature of the ordering is, if any. Diverse ground states can be realized as a result of the effects of chemical and physical pressure on the electronic structure. As correlations can play an important role in the determination of these ground states, it is important to understand their precise effect. Our work goes beyond the non-interacting and mean-field studies done previously and establishes not only the presence but also the stability of various topological phases and magnetic orders with the inclusion of strong correlations. Moreover, we predict that the axion insulator can in principle be realized due to the presence of a correlation-driven second order transition preceding a first order one. In this phase, the surface states are gapped and the magneto-electric effect exists even though the bulk is magnetically ordered. Generally, for both TI and axion phases, this suggests that a quantized magneto-electric response can be measured (by Kerr rotation for example [2]) even if other probes, such as optical conductivity or photoemission, point to the absence of sharp quasiparticles. It will be interesting to see if such indications for correlated topological phases can be found in the iridates or other materials. The methods used in our work, CDMFT (bulk and real space) and topological response computed using Green's functions, can be used for a wide class of complex oxides, not only those mentioned above. We suggest that these tools can be applied to examine generic interacting states with symmetry-protected topological order and combined with *ab initio* tools in the quest for experimentally relevant candidate materials.

We thank J.-M. Carter for his critical reading of the manuscript. This work was supported by the National Research Foundation of Korea (NRF) funded by the Korea government (MEST) through the Quantum Materials Research Center, No. 2011-0000982 and Basic Science Research, No. 2010-0010937 (AG, GSJ), NSERC, the Canada Research Chair program, and the Canadian Institute for Advanced Research (WWK, YBK), FQRNT and the Walter Sumner Foundation (WWK), NRF, No. 2008-0062238 (KP). The numerical computations were done in Seoul National University and SciNet at the University of Toronto.

Supplementary Material

Cellular dynamical mean-field theory

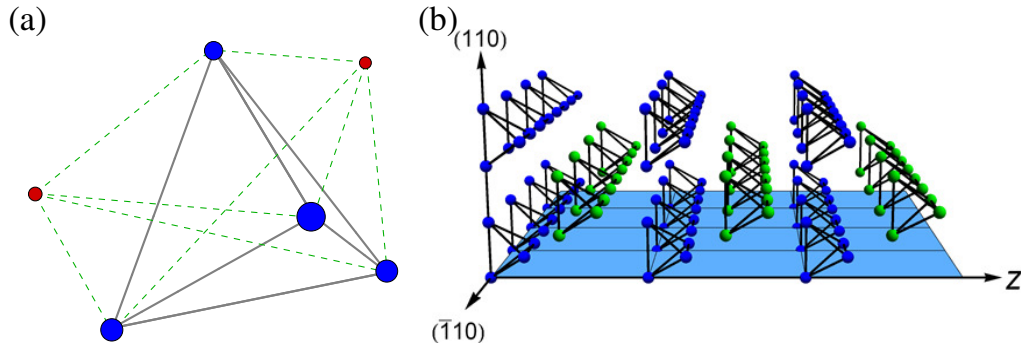


FIG. 4. CDMFT cluster and slab geometry. (a) Unit tetrahedron (cluster) and bath sites. Only $N_b = 2$ bath sites are shown while $N_b = 8$ (4) were used for the bulk and slab calculations, respectively. The blue and red spheres denote the cluster and the bath sites, respectively. The dashed green lines indicate the effective hybridization between the cluster and the bath. (b) Three layers within a slab that is finite along the (110)-direction. The tetrahedra in each layer are colored alternately with blue or green. We use 16 layers with periodic boundary conditions for the other two directions which span the sky-blue plane.

Cellular dynamical mean-field theory (CDMFT) [6, 7] reduces infinite lattice to a cluster of size N_c which hybridizes with the self-consistent electronic bath sites. It extends single-site DMFT with the goal of capturing spatial correlations more adequately. In this work, we use a tetrahedron cluster with 4 sites, which corresponds to a unit cell of the pyrochlore lattice. Figure 4 illustrates the cluster which is embedded in an effective, self-consistent bath. In order to investigate the ground state properties, we employ exact diagonalization to fully solve the quantum many-body properties of the cluster. The algorithm is iterative in nature: we initially input an ansatz for the bath parameters and solve the hybridized Hamiltonian with the impurity solver. From the cluster Hamiltonian we compute the cluster Green function \hat{G} , the hat denoting an 8×8 matrix structure, as well as the cluster self-energy, $\hat{\Sigma}^c = \hat{G}^{-1} - \hat{G}^{-1}$, where \hat{G} is the Weiss field describing the noninteracting bath. The new Weiss field is obtained by the self-consistent equation, $\hat{G}_{\text{new}}^{-1} = \hat{G}_{\text{loc}}^{-1} + \hat{\Sigma}^c$, where the local Green's function

$$\hat{G}_{\text{loc}}(i\omega_n) = \sum_{\mathbf{k}} \left[(i\omega_n + \mu)\hat{1} - \hat{t}(\mathbf{k}) - \hat{\Sigma}^c(i\omega_n) \right]^{-1} \quad (3)$$

is calculated by integration over the momentum vector of the reduced Brillouin zone (BZ). We then determine new bath parameters to best fit \hat{G}_{new} . The steps are repeated until convergence is reached.

The calculation for a slab structure is similar to the bulk case, but the Green's function is now an $8L \times 8L$ matrix. The self-consistent equation for a slab with L layers is given by

$$\mathcal{G}_{0,\text{new}}^{-1}(i\omega_n) = \left[\sum_{k_x, k_y} \frac{1}{(i\omega_n + \mu)\mathbf{1} - \mathbf{t}(k_x, k_y) - \mathbf{\Sigma}(i\omega_n)} \right]^{-1} + \mathbf{\Sigma}(i\omega_n), \quad (4)$$

where bold letters denote an $8L \times 8L$ matrix structure and the summation runs over the surface Brillouin zone. We assume that the self-energy is block-diagonal with the blocks of size eight. The correlations beyond a unit cell are treated on the mean-field level. In other words, the sectors make an effect on each other via the hopping matrix \mathbf{t} , although each sector of the self-energy is self-consistently determined by its own cluster Hamiltonian,

$$H_c^p = \sum_{\mu\nu\sigma} E_{\mu\nu}^p c_{p,\mu\sigma}^\dagger c_{p,\nu\sigma} + U \sum_{\mu} n_{p,\mu\uparrow} n_{p,\mu\downarrow} + \sum_{\mu l \sigma} (V_{p,\mu l \sigma}^p a_{p,l\sigma}^\dagger c_{p,\mu\sigma} + \text{h.c.}) + \sum_{l\sigma} \epsilon_{l\sigma}^p a_{p,l\sigma}^\dagger a_{p,l\sigma}, \quad (5)$$

where $\mu, \nu = 1, 2, \dots, 4$ are the site indices in a unit cell, $l = 1, 2, \dots, N_b$ label the bath sites, and $p = 1, \dots, L$ is a

layer index. The hoppings within a cluster and chemical potential are introduced by \hat{E} while the L -effective Weiss fields are described by the V 's and ϵ 's.

Topological invariant Δ

We provide information on the implementation of the topological invariant Δ [20] and its usage in the absence of TRS. For clarity, we rewrite it here,

$$(-1)^\Delta = \prod_{\text{R-zero}} \eta_\alpha^{1/2}. \quad (6)$$

As was noted in the main text, $\eta_\alpha = \pm 1$ is a parity eigenvalue corresponding to an eigenstate, $|\alpha\rangle$, of the (inverse) of the interacting Green's function, evaluated at one of eight TRIM, Γ_i . We now explain the notion of ‘‘Right-zero’’ (R-zero). The eigenvector satisfies:

$$\hat{G}^{-1}(i\omega, \Gamma_i) |\alpha(\omega, \Gamma_i)\rangle = \mu_\alpha(\omega, \Gamma_i) |\alpha(\omega, \Gamma_i)\rangle, \quad (7)$$

$$\hat{P} |\alpha(\omega, \Gamma_i)\rangle = \eta_\alpha |\alpha(\omega, \Gamma_i)\rangle, \quad (8)$$

where $\hat{G}^{-1}(i\omega, \mathbf{k})$ is the inverse Green's function, $\mu_\alpha(\omega, \mathbf{k})$ is its generally complex eigenvalue, and \hat{P} the parity operator. For fixed \mathbf{k} , as ω is tuned from $-\infty$ to ∞ , $\mu_\alpha(\omega, \mathbf{k})$ sweeps a curve in the complex plane. At $\omega = 0$, $\hat{G}^{-1}(0, \mathbf{k})$ is Hermitian hence its eigenvalues are real. Thus, $\mu_\alpha(0, \mathbf{k})$ crosses the real axis in the complex plane and in this sense is called a ‘‘zero’’. It is a R-zero simply if the crossing occurs to the right of the imaginary axis, i.e.

$$\text{R-zero} \Leftrightarrow \mu_\alpha(0, \mathbf{k}) > 0. \quad (9)$$

Hence, if $\mu_\alpha(0, \Gamma_i)$ is a R-zero, the associated parity eigenvalue η_α will contribute to the product for $(-1)^\Delta$ above.

In the presence of TRS, each $|\alpha(0, \Gamma_i)\rangle$ has a time-reversal partner with the same eigenvalue μ_α [20]. Each of these Kramers pairs of odd-parity eigenstates contributes $i^2 = -1$, and the index can only be zero or one. When one breaks TRS, the R-zeroes need not come in Kramers pairs. However, we argue that even in that case, as long as inversion symmetry is preserved, the topological index can still be used to test for the presence of a quantized magneto-electric response. An insulator with TRS broken but with such a response is called an axion insulator [8, 21]. The applicability of Δ for such inversion-symmetric topological insulators was briefly suggested in Ref. [20].

When TRS is broken, one needs to first ensure that Δ remains 0 or 1, avoiding imaginary values for instance. The equivalent statement for band insulators was established in references [21, 22], where it was shown that inversion symmetric band insulators always have an even number of odd-parity occupied states (including all TRIM). For correlated inversion-symmetric insulators, this would translate to the requirement to have an even number of odd-parity R-zeroes. This property is expected for insulators that are adiabatically connected to a band-insulator. With this constraint, we can write an equivalent expression for Δ :

$$\Delta = \frac{N_o}{2} \pmod{2}, \quad (10)$$

where N_o is the total (even) number of odd-parity R-zeroes at the TRIM. This formula also applies to the TRS case. In other words, for an insulator, a necessary condition to have a topologically non-trivial magneto-electric response is that N_o be twice an odd number. In the presence of TRS it is sufficient and we have the TI discussed above. Otherwise, one also needs to ascertain that the Hall conductivities vanish [21].

We describe the evolution of the parities, and hence of Δ , as we increase U in the TI, see Table I. At $U = 0$, we have a topological band insulator and Eq. (6) reduces to the Fu-Kane index, ν_0 [30]. Indeed, the condition of being a R-zero then implies an occupied Bloch state at the given TRIM. For $U > 0$, we use the interacting Green's function to compute Δ and find that its parity structure does not change as long as the state remains insulating. This must be so as the gap does not close, hence none of the eigenvalues of $\hat{G}^{-1}(0, \Gamma_i)$ can vanish. Eventually, TRS is spontaneously broken but continuously. For small values of the magnetization, not surprisingly, the parity structure is not affected and we have an axion insulator. The magnetization jumps at the first order transition. The large magnetization after the transition alters number of odd-parity R-zeroes at the L points such that $\Delta = 0$ because $N_o = 2 \times 6$. Strictly speaking, one should not evaluate Δ near the transition as the system is gapless there, being in a TWS phase. Eventually, a gap opens leaving behind a trivial antiferromagnetic insulator (AFI).

TABLE I. Number of odd-parity R -zeroes per TRIM. The non-trivial Green's function topology characterizes the topological insulator (TI) and axion insulator (AI) phases. A topological transition occurs as the system enters the gapless TWS. The change happens at the four L points.

U	Phase	Γ	X, Y, Z	L'	$L(\times 3)$	N_o
0.00	TI	0	2	4	0	10
3.00	TI	0	2	4	0	10
6.00	AI	0	2	4	0	10
6.11	TWS	0	2	3	1	12
8.00	AFI	0	2	3	1	12

-
- [1] M. Z. Hasan and C. L. Kane, Rev. Mod. Phys. **82**, 3045 (2010).
[2] X.-L. Qi and S.-C. Zhang, Rev. Mod. Phys. **83**, 1057 (2011).
[3] A. M. Turner, Y. Zhang, and A. Vishwanath, Phys. Rev. B **82**, 241102 (2010).
[4] X.-L. Qi, T. L. Hughes, and S.-C. Zhang, Phys. Rev. B **78**, 195424 (2008).
[5] Z. Wang, X.-L. Qi, and S.-C. Zhang, Phys. Rev. Lett. **105**, 256803 (2010).
[6] G. Kotliar, S. Y. Savrasov, G. Pálsson, and G. Biroli, Phys. Rev. Lett. **87**, 186401 (2001).
[7] T. Maier, M. Jarrell, T. Pruschke, and M. H. Hettler, Rev. Mod. Phys. **77**, 1027 (2005).
[8] X. Wan, A. M. Turner, A. Vishwanath, and S. Y. Savrasov, Phys. Rev. B **83**, 205101 (2011).
[9] L. Balents, Physics **4**, 36 (2011).
[10] A. A. Burkov and L. Balents, Phys. Rev. Lett. **107**, 127205 (2011).
[11] K.-Y. Yang, Y.-M. Lu, and Y. Ran, Phys. Rev. B **84**, 075129 (2011).
[12] D. Pesin and L. Balents, Nature Phys. **6**, 376 (2010).
[13] B.-J. Yang and Y. B. Kim, Phys. Rev. B **82**, 085111 (2010).
[14] M. Kargarian, J. Wen, and G. A. Fiete, Phys. Rev. B **83**, 165112 (2011).
[15] W. Witczak-Krempa and Y. B. Kim, Phys. Rev. B **85**, 045124 (2012).
[16] W. Witczak-Krempa, T. P. Choy, and Y. B. Kim, Phys. Rev. B **82**, 165122 (2010).
[17] G. Kotliar, S. Y. Savrasov, K. Haule, V. S. Oudovenko, O. Parcollet, and C. A. Marianetti, Rev. Mod. Phys. **78**, 865 (2006).
[18] B. J. Kim, H. Ohsumi, T. Komesu, S. Sakai, T. Morita, H. Takagi, and T. Arima, Science **323**, 1329 (2009).
[19] W. Wu, S. Rachel, W.-M. Liu, and K. Le Hur, (2011), arXiv:1106.0943.
[20] Z. Wang, X.-L. Qi, and S.-C. Zhang, (2012), arXiv:1201.6431v2.
[21] A. M. Turner, Z. Yi, R. S. K. Mong, and A. Vishwanath, (2010), arXiv:1010.4335v2.
[22] T. L. Hughes, E. Prodan, and B. A. Bernevig, Phys. Rev. B **83**, 245132 (2011).
[23] D. Yanagishima and Y. Maeno, J. Phys. Soc. Jpn. **70**, 2880 (2001).
[24] F. F. Tafti, J. J. Ishikawa, A. McCollam, S. Nakatsuji, and S. R. Julian, (2011), arXiv:1107.2544.
[25] S. Zhao, J. M. Mackie, D. E. MacLaughlin, O. O. Bernal, J. J. Ishikawa, Y. Ohta, and S. Nakatsuji, Phys. Rev. B **83**, 180402 (2011).
[26] K. Tomiyasu, K. Matsuhira, K. Iwasa, M. Watahiki, S. Takagi, M. Wakeshima, Y. Hinatsu, M. Yokoyama, K. Ohoyama, and K. Yamada, (2011), arXiv:1110.6605.
[27] M. C. Shapiro, S. C. Riggs, M. B. Stone, C. R. d. l. Cruz, S. Chi, A. A. Podlesnyak, and I. R. Fisher, (2012), arXiv:1201.5419.
[28] S. M. Disseler, C. Dhital, T. C. Hogan, A. Amato, S. R. Giblin, C. d. Cruz, A. Daoud-Aladine, S. D. Wilson, and M. J. Graf, (2012), arXiv:1201.4606.
[29] T. F. Qi, O. B. Korneta, X. Wan, and G. Cao, (2012), arXiv:1201.0538.
[30] L. Fu and C. L. Kane, Phys. Rev. B **76**, 045302 (2007).